Direct Evidence for the Role of the Madelung Potential in Determining the Work Function of Doped Organic Semiconductors

Perq-Jon Chia,[1] Sankaran Sivaramakrishnan,[1] Mi Zhou,[1] Rui-Qi Png,[1] Lay-Lay Chua,[1,2,*] Richard H. Friend,[1,3,†] and Peter K. H. Ho[1,‡]

[1]*Department of Physics, National University of Singapore, Lower Kent Ridge Road, Singapore 117542, Singapore*
[2]*Department of Chemistry, National University of Singapore, Lower Kent Ridge Road, Singapore 117543, Singapore*
[3]*Cavendish Laboratory, University of Cambridge, JJ Thomson Road, Cambridge CB3 0HE, United Kingdom*

(Received 16 September 2008; published 4 March 2009)

The work function of a model degenerately doped organic semiconductor *p*-doped poly(3,4-ethylenedioxythiophene)–poly(styrenesulfonic acid) can be systematically tuned over an eV-wide range by exchanging excess matrix protons with spectator cations, without altering the organic semiconductor doping level or polaron density. Ultraviolet photoelectron spectroscopy reveals this to arise not from an interface dipole, but from a bulk effect due to a shift in the Madelung potential set up by the local counter- and spectator-ion structure at the polaron sites. Electrostatic modeling of this potential is in agreement with the observed shift in carrier energetics. The spectator cations also cause a systematic shift in electron-phonon coupling and carrier delocalization, as revealed by infrared and Raman phonon modes, and charge-modulated absorption, which can be related to disorder in this potential.

DOI: 10.1103/PhysRevLett.102.096602 PACS numbers: 72.80.Le, 78.40.Me

The vacuum work function ϕ_{vac} is the difference in energy between carriers at Fermi level E_F and vacuum level E_{vac}. This quantity is fundamental to charge-carrier energetics and device injection barriers not only in traditional band-type semiconductors, but also in hopping-type π-conjugated organic semiconductors (OSCs) even though details of their E_F and carrier transport levels are still emerging [1]. It is well accepted that ϕ_{vac} is the sum of the carrier electrochemical potential ε and the interface dipole voltage Δ_{interf} through which the carrier has to cross: $\phi = \varepsilon + \Delta_{\mathrm{interf}}$ [2]. Recent work shows that Δ_{interf} depends on details of interface charge transfer [3], electrostatic dipole [4], and chemical bonding [5], while ε is a bulk property related to the OSC, polarity of doping [6,7], and doping level [8,9]. The role of the counterions, which charge-compensate the polaron charges on the doped OSCs, in determining this ε has yet to be clarified. In traditional semiconductors, these dopant ions are screened by the high dielectric constant of the crystal and so play no role in carrier energetics. However, this is not the case in OSCs, which are characterized by low local static dielectric constants ($\approx$3–6), high polaron densities ($\approx 10^{20}$ cm^{-3}), and strong carrier self-localization.

We demonstrate here through a systematic study of a family of *p*-doped OSCs with different spectator ions that ε is strongly influenced by the Madelung potential of the local ion structure. This can be modified through the ion-distance effect to alter work function over an eV-wide range without changing the OSC or its interface. Therefore control of this Madelung potential provides a new opportunity to tune carrier injection, extraction, and possibly exciton dissociation central to a variety of devices including photovoltaics, and also in biological systems.

The model OSC used here is the poly(3,4-ethylenedioxythiophene)–polystyrenesulfonate (PEDT:PSS) system. The parent PEDT:PSSH is the most well-characterized hole h^+ conductor to date [10]. This comprises *p*-doped PEDT chains of doping $\approx 0.3h^+$/ring [11] and chain length $\approx$12–20 rings/chain [12] dispersed in a matrix of polystyrenesulfonate PSS^- ions and poly(styrenesulfonic acid) PSSH. The holes are charge compensated by PSS^-, while the excess PSSH with ionizable protons (H^+) provides for water solubility [10]. By replacing the excess H^+ with monovalent ions (M^+) to generate a family of PEDT:PSSM daughters, we could systematically study the dependence of ϕ_{vac} and carrier energetics on the spectator M^+ without altering the fundamental chain length, doping level, or network morphology of the PEDT core.

We prepared the PEDT:PSSM daughters by ion-exchange dialysis of H^+ with M^+ at near neutral *p*H values in order to avoid dedoping the PEDT core [11,13]. In contrast, hydroxide neutralization causes chemical dedoping and degradation [14,15]. M^+ is thus a spectator that compensates the excess PSS^- in the polymer matrix. Alkali-metal cations (M = Li, ..., Cs) and tetraalkylammonium cations [M = tetramethylammonium (TMA), tetraethylammonium (TEA)] were studied. To do this, 1:2.5 mol/mol PEDT:PSSH (Baytron P, Leverkussen) solutions were dialyzed against M acetates (ionic strength $\approx 0.2M$) using a 12 kD-molecular-weight cutoff membrane, and purified by dialysis against Millipore water [11,13]. Ion exchange was better than 99% complete based on *p*H measurements. These PEDT:PSSM solutions were stable, 0.45-μm–filterable, and could be stored >1 y at room temperature without aggregation. The parent PEDT:

 © 2009 The American Physical Society

PSSH was also purified by dialysis against electronic-grade hydrochloric acid ($\approx 0.2M$) and then against Millipore water to remove ions and hydrolysis by-products [12]. All the studies here were thus performed on materials free from adventitious ion contamination.

Films were spin-cast in a class 1 k cleanroom and baked at 150 °C (hotplate) in the glovebox (pH_2O, $pO_2 <$ 1 ppm) to remove both physisorbed and coordinated water. This produces the dehydrated state, confirmed by x-ray photoelectron spectroscopy oxygen-to-sulfur atomic ratio ≈ 3.15 (theoretical 3.0), which is the standard state in OSC devices. In the dehydrated state, PSSH is un-ionized; i.e., the sulfonic acid group exists as $-SO_2OH$ [confirmed by Fourier-transform infrared spectrometry (cm^{-1}): $\nu_{as}SO_2 = 1352$; $\nu_sSO_2 = 1173$; $\nu OH = 909$], which provides a polar but nonionic matrix in which the $PEDT^+$ segments are distributed. On the other hand, PSSM ($M \neq H$) is always ionic, i.e., the sulfonate group exists as $-SO_{3^-} \cdots M^+$ ($\nu_{as}SO_{3^-} = 1192$; $\nu_sSO_{3^-} = 1130$).

Figure 1(a) shows the systematic E_F shift by almost 1 eV for PEDT:PSSM films on Au substrates. E_F was determined from the Fermi step of a metal reference, and E_{vac} from the low-energy secondary electron cutoff of the sample. The shoulder at -8.25 eV arises from nondispersive MOs, identified by PM3 semiempirical quantum chemical calculations to be PEDT sulfur lone pair and PSS phenyl ring MOs, while PEDT π MOs lie at lower and CH σ MOs at higher energies. The expanded spectra in the vicinity of E_F [Fig. 1(b)] do not show a step but an abrupt takeoff, indicating a small but finite $D(E_F)$ for all these films. The h^+/ring doping level is confirmed to be nearly constant

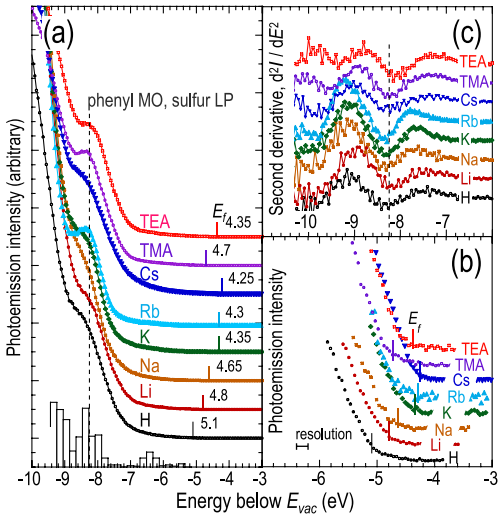

FIG. 1 (color online). UPS spectra of PEDT:PSSM thin films deposited on evaporated Au substrates, after annealing to 150 °C in N_2, probed by 21.21-eV HeI radiation. Sample bias, -10.00 V. No charging was found. (a) Valence band region, offset for clarity. Histogram bar gives the scaled density-of-states computed by the PM3 semiempirical method. (b) Expanded spectra of the spectra at E_F. (c) Second derivative spectra indicating energetic invariance (± 0.1 eV) of the valence MOs.

from the integrated intensity of the h^+ electronic spectra, and also from the absence of the 1.4 and 2.0 eV transitions characteristic of lightly p-doped and undoped PEDT, respectively, [Fig. 2(c)] [16,17].

The data rule out any change in the interface dipole causing an associated change in ϕ_{vac}. This is because the valence MOs and core levels do not shift in tandem with E_F referenced to E_{vac}, as shown explicitly for the S lone pair and phenyl MOs with similar photoemission kinetic energies as E_F [Figs. 1(b) and 1(c)]. The nonionic core levels (e.g., the C_{1s} and PEDT S_{2p}) are also constant to within ± 0.1 eV referenced to E_{vac}.

The origin of the E_F shift lies in the differential Madelung stabilization of h^+ polarons on the p-doped PEDT. This h^+-site energy can be written as $\varepsilon_i = \varepsilon_{chem} + eV_{M,i}$, where ε_{chem} is the chemical contribution and $V_{M,i}$ is the Madelung potential at site i, given by

$$V_{M,i} = -\frac{e^2}{4\pi\varepsilon_0\varepsilon_r}\sum_j \frac{q_j}{|r_j - r_i|}.$$

We supposed the ionic charges are confined to the interchain space between the hydrophobic PSS cores [Fig. 2(a), top] as in ionomers [18], in which the ions are locally ordered into multiplets with short-range layering of opposite ions [19,20]. Such a local order is also characteristic of other amorphous ionic systems, including molten binary salts [21] and ionic liquids [22]. Therefore we analyzed several local ion structure models in the hard-sphere approximation with overall charge neutrality. Figure 2(a) (bottom) shows, for example, a close-packed octapole structure (C_{3v} symmetry) in which the h^+ polaron contacts four close-packed sulfonates in a tetrahedron with one M^+ nested in each of the three hemi-octahedral holes. Its Madelung energy can be readily evaluated from

$$V_{M,i} = \frac{\alpha e^2}{4\pi\varepsilon_0}\sum_{j=1}^{7} \frac{q_j}{|r_j - r_i|},$$

where all distances to the h^+ were computed from known ionic radii [23], and α is a global scaling factor to accommodate geometric distortion, h^+ delocalization (which averages $V_{M,i}$), and an effective ε_r^{-1}. This Madelung sum has thus zero free parameters, aside from α which is of order unity <1 and constant within a structural family.

We also considered other high-symmetry ion structure models: an open C_{3v} octapole with four sulfonates and three M^+ at the vertices of a cubic lattice and h^+ at the last (distorted) vertex; a close-packed C_{2v} quadrupole with two sulfonates and one M^+ close-packed together with h^+; and an open C_{2v} quadrupole in which these form a distorted square lattice. The true structure is likely a weighted average of these. It is not surprising that such small multiplets are adequate for this purpose: the size constraint imposed by the hydrophobic chain [19,20], together with rapid decay of the pair correlation [21,22], effectively suppresses any longer correlation. The ratio of M^+ to h^+ is $\approx$ 8–10, and so interaction between h^+-h^+ is far less

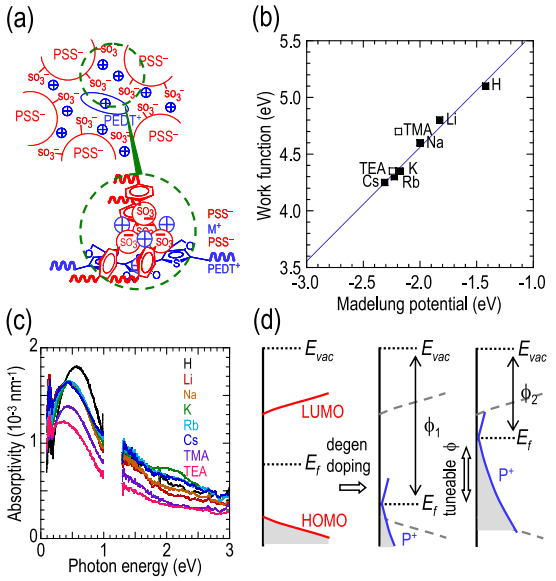

FIG. 2 (color online). Spectator-ion effects on the mean Madelung potential. (a) Schematic model of PEDT:PSSM, and a local ion octapole model with C_{3v} symmetry at the hole site. (b) Plot of the work function against the computed Madelung potential (see text). (c) Thickness-normalized transmission spectra of PEDT:PSSM films, ≈0.3-μm–thick on intrinsic Si for IR and ≈50-nm–thick on fused silica for the uv–visible–near-ir range. (d) Schematic diagram of the polaron density of states in doped OSCs emphasizing the variability of E_F with Madelung potential. Lowest unoccupied molecular orbital (LUMO); highest occupied molecular orbital (HOMO).

important than h^+-M^+. For PEDT:PSSH, we employed a single term in the Madelung sum which corresponds to the nearest-neighbor sulfonate ($d = 4.1$ Å, sum of the π-π half-thickness of 1.8 Å and anion r_- of 2.3 Å) as the next sulfonate is ≈15 Å away, similar to the next h^+.

Figure 2(b) shows the experimental ϕ_{vac} values plotted against the Madelung potential computed for the $M =$ Li, ..., Cs close-packed C_{3v} octapole and the $M =$ H dipole models. Negative potential corresponds to stabilization of h^+. We found a remarkable linear correlation ($R^2 = 0.985$) that gives unity slope (i.e., $d\phi/dV_M = 1$) for $\alpha = 0.48 \pm 0.03$, which is consistent with h^+ delocalization. The local ion structure is thus well described by these simple models. The data for $M =$ TMA and TEA also remarkably regress to this line for the same α value but in the lower-coordination close-packed C_{2v} quadrupole model. These quaternized ammonium ions are much larger (cation $r_+ = 3.22$ and 3.85 Å, respectively) than $Li^+, \ldots, Cs^+$ ($r_+ = 0.74, \ldots, 1.70$ Å) and the sulfonate, and so the lower coordination is not unexpected. The excellent agreement here affirms the importance of the local charge ordering: variations in the local ion distance and structure can generate eV-scale variation in V_M.

Previously we have demonstrated that interchain polaron interaction can produce a sufficient bandwidth for E_F holes to reside within an energy continuum [24]. Here it becomes clear that the Madelung potential plays a crucial role in determining the mean (and width) of this energetic distribution. Figure 2(d) gives a schematic illustration of this effect. Control of the density and nature of counter- and spectator-ions provides a way to achieve ultrahigh (or ultralow) work-function conductors suitable for hole (or electron) injection. It is also clear that the energetics of polarons electrochemically generated in the presence of counterions [9] can be shifted from those of carriers injected into devices in which such counterions are absent. Furthermore, doping-induced polarons at heterointerfaces should also experience different V_M than in the bulk.

This Madelung effect has several consequences. Because of disorder, V_M can be expected to fluctuate from site to site on the order of a fraction of an eV, as in liquid charge-transfer alloys [25], and contribute to h^+ pinning and localization. This should increase with decreasing r_+ (and hence decreasing $|V_M|$), because the V_M fluctuates more strongly with the positions of ions that are nearer. This fluctuation can be visualized through the oscillations in charge density and bond order of the PEDT chain, which increase as h^+ becomes more localized [26,27]. The increased oscillation for a given chain length and doping level suppresses on-chain phonon coupling and hence its dispersion, i.e., the change in frequency with wave vector. We examined the characteristic Raman-active ν_{2^+} (1500–1515 cm^{-1}), ν_{2^-} (≈1455–1460), ν_{3^+} and ν_{3^-} (≈1425–1445 cm^{-1}), and infrared-active (IRAV) ν_{CS} (≈830–845 cm^{-1}) skeletal modes that are not strongly admixed with vibrations of the ethylenedioxy bridge. We computed the conjugation length n dependence of these modes for ethylenedioxythiophene oligomer (EDT_n) models [28]. These frequencies relate to those of the doped PEDT by a simple shift due to effective conjugation coordinate [29] or phonon propagator [30]. The experimental mode frequencies across the $M =$ H, Li, ..., Cs series [Fig. 3(a)] are found to parallel the effect of increasing n [Fig. 3(b)]. Thus on-chain phonon coupling and h^+ delocalization increase across H, ..., Cs as predicted, which in fact is broadly consistent with the redshift of the population-averaged h^+ spectrum [Fig. 2(c)].

Electromodulated absorption (EA) spectroscopy of PEDT:PSSM films in ITO–50-nm PEDT:PSSM–105-nm polystyrene (PS)–Ca metal-insulator-metal capacitors [Fig. 3(c)] reveals a significant crossover in the site selectivity for electrostatic dedoping. No charge injection occurred into PS, so the EA response arises solely from modulation of the h^+ density of PEDT at the PS interface. This is confirmed by the absence of EA dependence on V_{dc} polarity across flatband potential, which differs from the usual Stark effect [31]. The EA absorption was in phase with the negative V_{ac}-half-cycle on PEDT, and so interface h^+ depletion has been directly observed here.

In the absence of counterions, this depletion should be statistically distributed owing to Coulomb repulsion

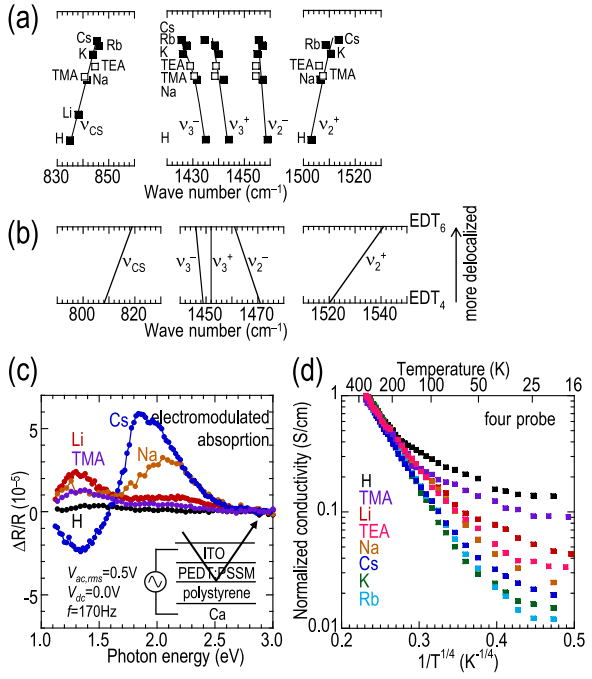

FIG. 3 (color online). Spectator-ion effects on phonon dispersion, electrostatic dedoping, and transport. (a) Experimental phonon mode frequencies of PEDT:PSSM, displaced for clarity on the ordinate axis. The mode frequencies were accurately obtained by second derivatives. (b) Computed mode dependence on chain length for ethylenedioxythiophene oligomers. (c) Electromodulated absorption spectra of ITO–50-nm PEDT:PSSM–105-nm polystyrene (PS)–Ca metal-insulator-metal capacitors measured in reflection. Voltage applied on PEDT relative to cathode. (d) Variable-temperature conductivity plots presented in the Mott variable-range ($T^{-1/4}$) representation.

[26,27]. For a modulation depth $\Delta\sigma = \frac{\varepsilon_0\varepsilon_r}{d} V_{\mathrm{ac}}$ of $\approx 1 \times 10^{-8}$ C cm^{-2} (i.e., $\approx$1% of a PEDT monolayer), this corresponds to $\ll 1 h^+$ per chain. For M = H as expected, the h^+ depletion produces a barely detectable lightly p-doped state [16,17] at 1.4 eV and no neutral state [16,17] at 2.0 eV. For M = Li, however, the neutral state which requires a correlated loss of a few h^+ from a single chain begins to emerge, while for M = Cs this completely dominates the spectrum. This crossover from uncorrelated to correlated h^+ depletion suggests an increased tendency for disproportionation with increased delocalization of the holes.

Finally, we considered whether the V_M fluctuation would lead to differences in the thermal activation of h^+ transport. Variable-temperature four-in-line probe measurements [Fig. 3(d)] reveal a universal behavior at high temperatures and a leveling off at low temperatures depending on M. Thus h^+ transport is not limited by V_M disorder, but perhaps by interchain coupling.

In summary, we have provided direct evidence for the role of the Madelung potential in determining the energetics of the conduction carriers in a doped organic semiconductor. This not only clarifies an important aspect of the work function of these mixed ion-electron systems, but also points to an important principle for the manipulation of their work function.

We acknowledge stimulating discussions with Jeremy Burroughes (CDT). This work was supported by MOE ARF (Project No. 144-000-131-112) and A*STAR SERC (Project No. 052-117-0030).

*phycll@nus.edu.sg
†rhf10@cam.ac.uk
‡phyhop@nus.edu.sg

[1] D. Cahen and A. Kahn, Adv. Mater. **15**, 271 (2003).
[2] S. Duhm *et al.*, Nature Mater. **7**, 326 (2008).
[3] N. Koch *et al.*, Phys. Rev. Lett. **95**, 237601 (2005).
[4] G. Heimel *et al.*, Phys. Rev. Lett. **96**, 196806 (2006).
[5] P. S. Bagus *et al.*, Phys. Rev. Lett. **100**, 126101 (2008).
[6] M. Lögdlund *et al.*, Phys. Rev. Lett. **63**, 1841 (1989).
[7] M. Fahlman *et al.*, Chem. Phys. Lett. **214**, 327 (1993).
[8] M. Gross *et al.*, Nature (London) **405**, 661 (2000).
[9] I. N. Hulea *et al.*, Phys. Rev. Lett. **93**, 166601 (2004).
[10] L. B. Groenendaal *et al.*, Adv. Mater. **12**, 481 (2000).
[11] P. J. Chia *et al.*, Adv. Mater. **19**, 4202 (2007).
[12] R. Q. Png *et al.*, Appl. Phys. Lett. **91**, 013511 (2007).
[13] L. L. Chua *et al.*, Adv. Mater. **16**, 1609 (2004).
[14] M. M. de Kok *et al.*, Phys. Status Solidi (a) **201**, 1342 (2004).
[15] C. H. L. Weijtens *et al.*, Org. Electron. **6**, 97 (2005).
[16] P. K. H. Ho *et al.*, Nature (London) **404**, 481 (2000).
[17] L. B. Groenendaal *et al.*, Adv. Mater. **15**, 855 (2003).
[18] J. J. Fitzgerald and R. A. Weiss, J. Macromol. Sci., Rev. Macromol. Chem. Phys. **C28**, 99 (1988).
[19] A. Eisenberg, Macromolecules **3**, 147 (1970).
[20] K. A. Mauritz, J. Macromol. Sci., Rev. Macromol. Chem. Phys. **C28**, 65 (1988).
[21] M. P. Torsi, Annu. Rev. Phys. Chem. **44**, 173 (1993).
[22] C. Hardacre *et al.*, J. Chem. Phys. **118**, 273 (2003).
[23] We computed $V_{M,i}$ using standard Shannon-Prewitt ionic radii for the alkali series. The radii for the other groups are given in the text.
[24] J. M. Zhuo *et al.*, Phys. Rev. Lett. **100**, 186601 (2008).
[25] T. Koslowski and D. E. Logan, J. Phys. Chem. **98**, 9146 (1994).
[26] A. J. W. Tol, Chem. Phys. **208**, 73 (1996).
[27] S. S. Zade and M. Bendikov, J. Phys. Chem. C **111**, 10 662 (2007).
[28] PM3 calculations were performed on geometry-optimized planar undoped EDT$_n$ oligomers, and frequency calibrated to the experimental results of D. Wasserberg *et al.*, J. Am. Chem. Soc. **128**, 17 007 (2006). Separate calculations on thiophene oligomers for which a wider set of data is available show that the same scaling reproduces experimental frequencies to $\pm$1%.
[29] J. T. Lopez Navarrete and G. Zerbi, J. Chem. Phys. **94**, 965 (1991).
[30] R. Österbacka *et al.*, Phys. Rev. Lett. **88**, 226401 (2002).
[31] V. Bodrozic *et al.*, Adv. Mater. **20**, 2410 (2008).